

Influence of orbital sets on the $\text{Ar}^+(2s^{-1})$ multiple Auger decay

Zhenqi Liu¹,^{*} Qing Liu,¹ Yulong Ma,² Fuyang Zhou,³ and Yizhi Qu^{1,*}

¹*School of Optoelectronics, University of Chinese Academy of Sciences, Beijing 100049, China*

²*College of Physics and Electronic Engineering, Northwest Normal University, Lanzhou 730070, China*

³*Data Center for High Energy Density Physics, Institute of Applied Physics and Computational Mathematics, Beijing 100088, China*



(Received 29 January 2021; revised 13 April 2021; accepted 14 May 2021; published 3 June 2021)

The single, double, triple, and quadruple Auger decays of $\text{Ar}^+(2s^{-1})$ are studied, based on many-body perturbation theory. The level-to-level investigation indicates that the double Auger primarily comes from the cascade process involving the Coster-Kronig decay. Moreover, the complex triple Auger and quadruple Auger decay are expressed by the multistep approach, i.e., the combination of cascade and direct processes. On the other hand, by employing the separate orbital sets for optimizing the single-electron wave functions, our ion yield ratios ($\text{Ar}^{2+} : \text{Ar}^{3+} : \text{Ar}^{4+} : \text{Ar}^{5+} = 3.5 : 88.7 : 7.5 : 0.26$) agree quite well with the recent experimental data (3:89:8:0.3) [Lablanquie *et al.*, *Phys. Chem. Chem. Phys.* **13**, 18355 (2011)]. Moreover, the single, double, and triple Auger spectra, as well as lifetime, are all in accord with the measurements of Lablanquie *et al.*

DOI: [10.1103/PhysRevA.103.063102](https://doi.org/10.1103/PhysRevA.103.063102)

I. INTRODUCTION

The Auger, especially the multiple Auger (MA) decay process with more than one emission electron when the outer electron fills the inner-shell vacancy, is of longstanding interest for experimental and theoretical studies [1–7]. Useful information can be drawn about the electron-electron correlations for different shell structures of atoms and ions from MA decay [4]. The significant MA spectra are widely utilized in material science [8], and the study of electronic structure of atoms and molecules [9]. The spectra contribute to elucidate the MA decay processes: the double-Auger (DA) decay [2] spectra are represented with the sum of direct and cascade processes; while, for the triple Auger (TA) and quadruple Auger (QA), their spectra are so complex that a more detailed analysis is required elaborately (see, e.g., Refs. [6,10,11] and references therein).

In the past few decades, the Auger decay of atoms especially the noble gases were investigated intensively [1,2,4,6,10–22], since the noble gases with closed shells are easy to obtain in experiments, and easier tests of the theoretical models by comparison with experiments [23]. The study of Ar Auger decay has lasted more than half a century [5,24]; moreover, Ar ions are of significance in astrophysical [25] and laboratory plasmas [26,27]. In this paper, we concentrate on the MA decay of $\text{Ar}^+(2s^{-1})$ as comprehensively as possible. Mehlhorn (1968) [5] conducted the first $\text{Ar}^+(2s^{-1})$ Auger decay. In the 1990s, Glans *et al.* [28], and Kylli *et al.* [29] further measured the Coster-Kronig spectra and lifetime experimentally. Kasstra *et al.* [30], and Kochur *et al.* [16] gave the ion yield ratios ($\text{Ar}^{2+} : \text{Ar}^{3+} = 3.6 : 96.4$) and ($\text{Ar}^{2+} : \text{Ar}^{3+} : \text{Ar}^{4+} = 4.2 : 93.4 : 2.5$) via Hartree-Fock calculation, respectively; however, the detailed MA spectra were not represented. The first more comprehensive experiment was done

by Brünken *et al.* [31] in 2002; using photoelectron-ion coincidence spectroscopy, they discussed the possible decay routes, and determined the ion yield ratios ($\text{Ar}^{2+} : \text{Ar}^{3+} : \text{Ar}^{4+} = 1 : 89 : 10$). In the latest experimental research of Lablanquie *et al.* [32,33] (2011, 2017), the MA decay process of $\text{Ar}^+(2s^{-1})$ up to the Ar^{5+} was explored in great detail using multielectron coincidence Auger spectroscopy, with the aid of magnetic bottle time of flight analyzer; the more complex decay processes were detected and indicated. Moreover, the ion yield ratios ($\text{Ar}^{2+} : \text{Ar}^{3+} : \text{Ar}^{4+} : \text{Ar}^{5+} = 3 : 89 : 8 : 0.3$), lifetime and SA, DA and TA spectra were also obtained.

It is obvious that the theoretical TA ratio of 2.5% [16] in $\text{Ar}^+(2s^{-1})$ Auger decay is distinctly below the experimental results of 8% [31] and 10% [32], respectively, and the TA ratio is absent in Ref. [30]. The absence of MA spectra and the deviation of ion yield ratios come from the difficulty to optimize the single-electron wave functions and distinguish the complex decay processes, especially for the TA and QA processes. In addition, the $\text{Ar}^+(2s^{-1})$ decay is mainly a Coster-Kronig Auger [16,29,31,32,34], where a higher subshell with the same shell as initial state hole fills the hole (e.g., $2s \rightarrow 2p$). It is a challenge for theoretical study; for such small transition energy, the accurate wave functions sensitive to the calculation methods are required. Further, changes in kinetic energies and potential, generated by the wave functions, would easily affect the Auger decay rates [35].

In this work, based on many-body perturbation theory, separate orbital sets are adopted to search for high-quality single-electron wave functions. Moreover, we employ the multistep approach including cascade, knock-out (KO), and shake-off (SO), as well as their combination to simulate the MA decay. In consequence, the SA, DA, and TA decay spectra, lifetime, and complete ion yield ratios are all consistent with the results of recent experiments [32,33].

The following parts of the paper are structured as follows. In Sec. II, the underlying theory of SA and DA decays is described. In Sec. III, the details of different approaches are

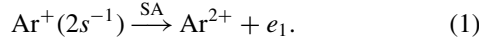
*yzqu@ucas.edu.cn

explained, the theory of TA and QA decays are given, and all MA results are compared with other theoretical and experimental investigations. Finally, a summary of the findings is drawn in Sec. IV.

II. THEORY

A. Single Auger decay

The $\text{Ar}^+(2s^{-1})$ can decay to Ar^{2+} , forming the single Auger (SA) process



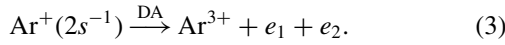
Its rate is given by [9,36]

$$A_{if}^{\text{SA}} = \left| \langle \psi_f^{2+}, \kappa; J_T M_T | \sum_{p < q} \frac{1}{r_{pq}} | \psi_i^+ \rangle \right|^2, \quad (2)$$

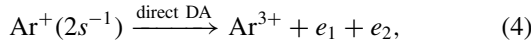
where $|\psi_i^+\rangle$ denotes the initial state $\text{Ar}^+(2s^{-1})$, and $|\psi_f^{2+}, \kappa; J_T M_T\rangle$ represents the final state Ar^{2+} plus a continuum Auger electron. κ , J_T , and M_T represent the relativistic angular quantum number of continuum Auger electron, the total angular momentum, and the magnetic quantum number of final states, respectively.

B. Double Auger decay

The $\text{Ar}^+(2s^{-1})$ can also decay to Ar^{3+} with the emission of two electrons, forming the double Auger (DA)



Since the initial state $\text{Ar}^+(2s^{-1})$ and final states Ar^{3+} differ by at least three single-electron wave functions, one cannot get the DA rates directly (see, e.g., Refs. [7,9,37]). Based on the many-body perturbation theory [3], the approximated formulas for calculating the DA rates including direct and cascade processes are obtained [2]. The direct process, accompanying with two Auger electrons emissions simultaneously, can be expressed as



which can be divided into two mechanisms: knock-out (KO) and shake-off (SO). The KO mechanism is a virtual inelastic scattering impact ionization process [3], and its rate is given by

$$A_{if}^{\text{DDA(KO)}} = \sum_m A_{im}^{\text{SA}} \Omega_{mf}(\varepsilon_{im}), \quad (5)$$

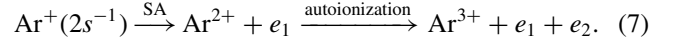
where A_{im}^{SA} denotes the SA rate; $\Omega_{mf}(\varepsilon_{im})$ represents the collision strength of the inelastic scattering upon the ‘‘intermediate’’ Auger state m to the final states Ar^{3+} .

The SO mechanism is a pure quantum effect in which the second Auger electron is ejected on account of the relaxation in which the atomic potential changes suddenly. Its rate can be written as

$$A_{if}^{\text{DDA(SO)}} = \sum_m A_{im}^{\text{SA}} |\langle \psi_f^{3+}, \kappa; J_T M_T | \psi_m^{2+} \rangle|^2, \quad (6)$$

where the matrix element $\langle \psi_f^{3+}, \kappa; J_T M_T | \psi_m^{2+} \rangle$ is the overlap integral between the intermediate state and final state.

The cascade mechanism for DA is a sequential two-step SA process. The $2p$ core electron fills the initial state $\text{Ar}^+(2s^{-1})$ along with the emission of primary Auger electron, producing the intermediate autoionization state Ar^{2+} ($2p^5 3s 3p^6$ and $2p^5 3s^2 3p^5$, etc.). Then, those autoionization states can undergo further SA decay, ultimately forming the final states Ar^{3+} . It can be described as



The rate of the cascade mechanism satisfies the equation following

$$A_{if}^{\text{DCA}} = \sum_m A_{im}^{\text{SA}} A_{mf}^{\text{SA}} \Gamma_m^{-1}, \quad (8)$$

where A_{im}^{SA} and A_{mf}^{SA} denote the Auger decay rate from the initial state $\text{Ar}^+(2s^{-1})$ to the intermediate autoionization state Ar^{2+} , and then to the final state Ar^{3+} . Γ_m represents the total width of the specific intermediate state m of Ar^{2+} .

Throughout this paper, the orbital sets for optimizing single-electron wave functions of each ion state are performed in the GRASP2K program [38]. The atomic state functions (ASFs) and the SA rates are computed utilizing the XRELCI and XAUGER components of the RATIP-2012 code [37], respectively. For the direct DA process, both the collision ionization strengths and the overlap integrals are obtained using the flexible atomic code (FAC) [36] with certain modifications [11]. The collision strength calculated from the FAC for the free-electron impact ionization is modified for the electron with certain momentum l , as shown in Eq. (5). In addition, the radiation process is neglected for its formation probabilities are much smaller than that of Auger decay by at least four orders of magnitude in this calculation.

III. RESULTS AND DISCUSSION

For the convenience of discussion, Fig. 1 exhibits the energy level diagram for the main decay processes of SA, DA, TA, and QA of $\text{Ar}^+(2s^{-1})$. The Ar^{2+} ion states come from

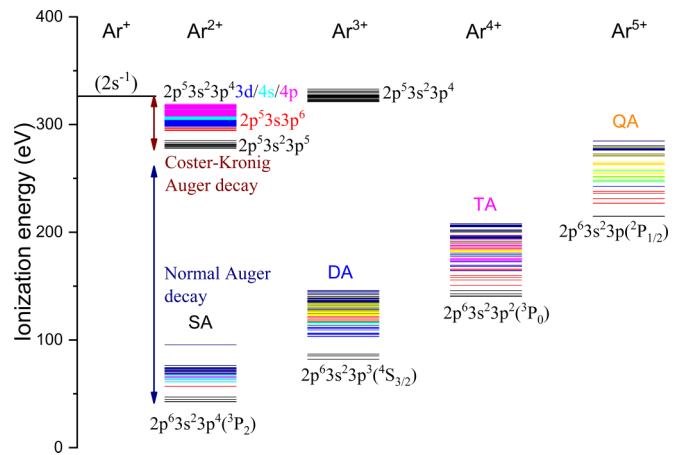


FIG. 1. Energy level diagram of Ar ions in reference to the ground state of Ar atom. The main configurations for the single Auger (SA), double Auger (DA), triple Auger (TA), and quadruple Auger (QA) decays of $\text{Ar}^+(2s^{-1})$ are presented. The Ar^{2+} ion states come from the Coster-Kronig and normal Auger decays.

TABLE I. The detailed choice of orbital sets and configuration interaction (CI) for each ion state in the calculation. In active orbitals, (S) and (D) indicate the single and double electron excitations, respectively. The Ar²⁺ involve the normal orbital sets (NOS) and separate orbital sets (SOS).

Ion states	Multiconfigurations for the orbital sets	CI		
		Reference configuration	Active orbitals	Active space
Ar ⁺ (2s ⁻¹)	{1s ² 2s2p ⁶ 3s ² 3p ⁶ }	{1s ² 2s2p ⁶ 3s ² 3p ⁶ }	SD {3s, 3p}	{3d, 4s, 4p}
Ar ²⁺ (NOS)	{2p ⁶ 3s ² 3p ⁴ , 2p ⁶ 3s3p ⁵ , 2p ⁶ 3p ⁶ }	{2p ⁶ 3s ² 3p ⁴ , 2p ⁶ 3s3p ⁵ }	SD {3s, 3p} and S {2p}	{3d, 4s, 4p}
Ar ²⁺ (SOS ^a)	{Normal Auger {2p ⁶ 3s ² 3p ⁴ , 2p ⁶ 3s3p ⁵ , 2p ⁶ 3p ⁶ } {Coster-Kronig {2p ⁵ 3s ² 3p ⁵ , 2p ⁵ 3s3p ⁶ }}	{2p ⁶ 3s ² 3p ⁴ , 2p ⁶ 3s3p ⁵ }	SD {3s, 3p}	{3d, 4s, 4p}
		{2p ⁵ 3s ² 3p ⁵ , 2p ⁵ 3s3p ⁶ }	SD {3s, 3p}	{3d, 4s, 4p}
Ar ³⁺	{2p ⁶ 3s ² 3p ³ , 2p ⁶ 3s3p ⁴ }	{2p ⁶ 3s ² 3p ³ , 2p ⁶ 3s3p ⁴ }	SD {3s, 3p}	{3d, 4s, 4p}
A ⁴⁺	{2p ⁶ 3s ² 3p ² , 2p ⁶ 3s3p ³ }	{2p ⁶ 3s ² 3p ² , 2p ⁶ 3s3p ³ }	SD {3s, 3p}	{3d, 4s, 4p}
A ⁵⁺	{2p ⁶ 3s ² 3p, 2p ⁶ 3s3p ² }	{2p ⁶ 3s ² 3p, 2p ⁶ 3s3p ² }	SD {3s, 3p}	{3d, 4s, 4p}

^aThe SOS is that the orbitals of Coster-Kronig and normal Auger decay final states are optimized separately in Ar²⁺.

two parts: the Coster-Kronig SA decay whereby 2p core-hole electron fills the 2s core hole with the emission of valence electron (3s or 3p) forming Ar²⁺ ion states such as 2p⁵3s²3p⁵, 2p⁵3s3p⁶, around the 290 eV, and the normal SA decay whereby the valence electrons take part in the filling and emission forming Ar²⁺ ion states such as 2p⁶3s²3p⁴, 2p⁶3s3p⁵ around 50 eV in Fig. 1. For the Coster-Kronig decay, the transition energies between initial state Ar⁺(2s⁻¹) and final states Ar²⁺ 2p⁵3s²3p⁵ states are about 50 eV, while, in the normal SA decay, the transition energies are about 280 eV. The different transition energies in the Coster-Kronig decay and normal SA decay are manifest in the huge ionization energy difference between the 2p and 3p of Ar²⁺. As for Ar³⁺, some levels of 2p⁵3s²3p⁴ are below the level of initial state; then Ar⁺(2s⁻¹) has the possible decay to Ar³⁺ (2p⁵3s²3p⁴).

A. Single Auger decay

First, we consider the SA decay of Ar⁺(2s⁻¹), for its rates are significant and have a direct connection with the results of MA. The orbitals of the initial and final states (Ar⁺–Ar²⁺) are optimized separately, taking the relaxation effect into account. In addition, the nonorthogonality between the orbitals of initial states and final states does not affect the Auger results in the Ar⁺(2s⁻¹) decay (see, e.g., Refs. [11,37,39,40]) obviously in comparison with the resonant Auger decay [9,10], for the impact of shake process is limited in the Ar⁺(2s⁻¹) decay. The multiconfigurations for the orbital sets, and CI, in initial states Ar⁺(2s⁻¹), the normal orbital sets (NOS) and separate orbital sets (SOS) of Ar²⁺, as well as the Ar³⁺, Ar⁴⁺, Ar⁵⁺, are listed in Table I.

The calculations are based on the multiconfiguration Dirac-Fock (MCDF). The initial state orbitals of Ar⁺(2s⁻¹) are achieved by optimizing the orbital set of single configuration 1s²2s2p⁶3s²3p⁶. The reason for the selection of single configuration is that we just focus on the state of Ar⁺(2s⁻¹). Note that the multiconfiguration is adopted in the final states of Ar²⁺–Ar⁵⁺ below, since we should take into account all the main decay configurations.

The aim of CI is to contain more configuration state functions (CSFs) to better consider the electronic correlation effect, based on the obtained orbitals. The CI is extended using the active set approach that the valence orbitals 3s, 3p (active

orbitals) single and double excite from reference configuration 1s²2s2p⁶3s²3p⁶ to active space of 3d, 4s, 4p.

For the optimization of Ar²⁺ states, we employ the NOS that all the ASFs are obtained by optimizing the same orbital sets of configurations, which is a common practice in Auger decay [10,11,41]. In the MCDF calculation, the orbital sets of Ar²⁺ multiconfigurations are 2p⁶3s²3p⁴, 2p⁶3s3p⁵, and 2p⁶3p⁶. The CSFs of the CI expansion include the single and double excitations of 3s, 3p orbitals and the single excitations of 2p extended from reference configurations 2p⁶3s²3p⁴ and 2p⁶3s3p⁵ to the active space of 3d, 4s, 4p.

Our theoretical normal SA spectra well simulate the experimental results [32], as shown in Fig. 2, covering the kinetic energy range from 230 to 300 eV. On the basis of the energy-resolving power of the apparatus $\Delta E/E \approx 1.5\%$ in the experiment [32], our spectra are convolved with a Gaussian profile of 4 eV full width at half maximum (FWHM) for the Auger electron around 267 eV. 2p⁶3s3p⁵ and its satellite 2p⁶3s²3p³3d represent the two strongest peaks, taking

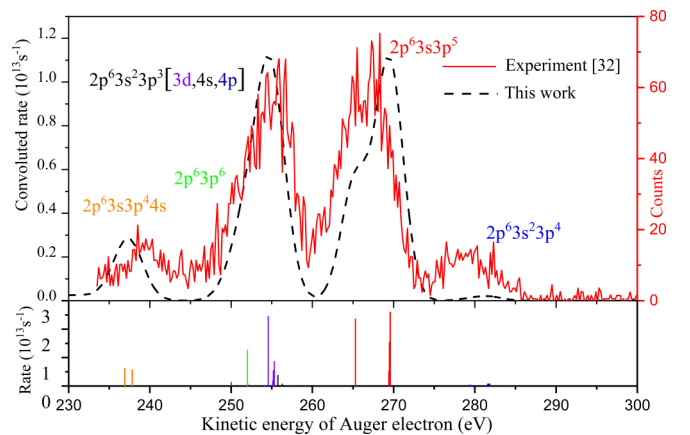


FIG. 2. Comparison of the normal SA spectra. The y axis of the experimental Auger spectra corresponds to the measured counts. For comparison, our theoretical transition rates are convolved with a Gaussian profile of 4 eV FWHM, and the spectra are normalized to the main peak of experimental results (the same as below Figs. 3–6). The vertical solid lines with different colors below the figure correspond to different final-state transition rates.

TABLE II. Rates (A) and branching ratios (BRs) for the normal SA main transition configuration and levels in normal orbital sets (NOS) and separate orbital sets (SOS). The decay of SA corresponds to Eq. (1). The numbers in parentheses denote powers of 10.

Ar ²⁺		NOS		SOS	
Configuration	Level	$A(s^{-1})$	BR (%)	$A(s^{-1})$	BR (%)
$2p^63s^23p^4$		1.07(12)	0.8	1.08(12)	0.8
$2p^63s3p^5$		7.03(13)	52.5	6.97(13)	52.0
	3P_2	2.61(13)	19.5	2.60(13)	19.4
	3P_1	1.54(13)	11.5	1.54(13)	11.5
	3P_0	5.15(12)	3.8	5.14(12)	3.8
	1P_1	2.37(13)	17.7	2.32(13)	17.3
$2p^63s^23p^33d$		4.33(13)	32.3	4.37(13)	32.6
$2p^63s^23p^34s$		4.94(12)	3.7	4.60(12)	3.4
$2p^63s^23p^34p$		1.50(12)	1.1	2.10(12)	1.5
$2p^63p^6$		1.27(13)	9.5	1.24(13)	9.3
Total		1.34(14)	100	1.33(14)	100

up most part of the total ion yields. The underestimation of $2p^63s^23p^4$ maybe come from the double photoionization of (Ar - Ar²⁺), and further analysis is necessary.

For the detailed analysis of the normal SA, the rates and branching ratios (BRs) of main transition configurations and states are listed in Table II. The intensities of $2p^63s3p^5$ are foremost, accounting for about 52.5% of normal SA transition rates, of which the contributions of triplet state $^3P_{2,1,0}$ are larger than that of single-state 1P_1 . Due to the strong mixing with $2p^63s3p^5$, the $2p^63s^23p^33d$ are contributed to total rates considerably, with about 32.3%. These indicate that in the normal SA, mainly one $3s$ electron fills the $2s$ hole with the emission of a $3p$. While configurations $2p^63s^23p^4$, $2p^63s^23p^34s$, $2p^63s^23p^34p$, and $2p^63p^6$ play a minor role, compared with those of $2p^63s3p^5$ and $2p^63s^23p^33d$.

Now we come to consider the Coster-Kronig Auger decay. The theoretical spectra convolved via a Gaussian profile of 2.25 eV FWHM are compared with the experimental results [32] in Fig. 3, with the kinetic energy range of Auger electron from 0–55 eV. The difference between the two spectra is obvious.

These differences may come from the choice of the orbital sets or the CI expansion. As shown in Fig. 1, the energy difference between final states of normal Auger decay ($2p^63s^23p^4$, etc.) and the Coster-Kronig decay states with $2p$ hole ($2p^53s^23p^5$, etc.), are more than 200 eV. In order to study the influence of both normal and Coster-Kronig Auger, the approach of separate orbital sets, in which the Coster-Kronig and normal Auger decay orbitals are optimized separately, is introduced.

Then we introduce the separate orbital sets (SOS), as shown in Table I, in which the ASFs of Ar²⁺ states are obtained with two separate parts: for the normal Auger decay final states, the orbital sets are obtained from the same multiconfigurations as NOS, i.e., Ar²⁺ $2p^63s^23p^4$, $2p^63s3p^5$, and $2p^63p^6$; for the Coster-Kronig decay final states, the multiconfigurations Ar²⁺ $2p^53s^23p^5$ and $2p^53s3p^6$ are selected for orbital sets. In both cases, the CI is extended on the basis of valence orbitals $3s$, $3p$ single and double excitation from

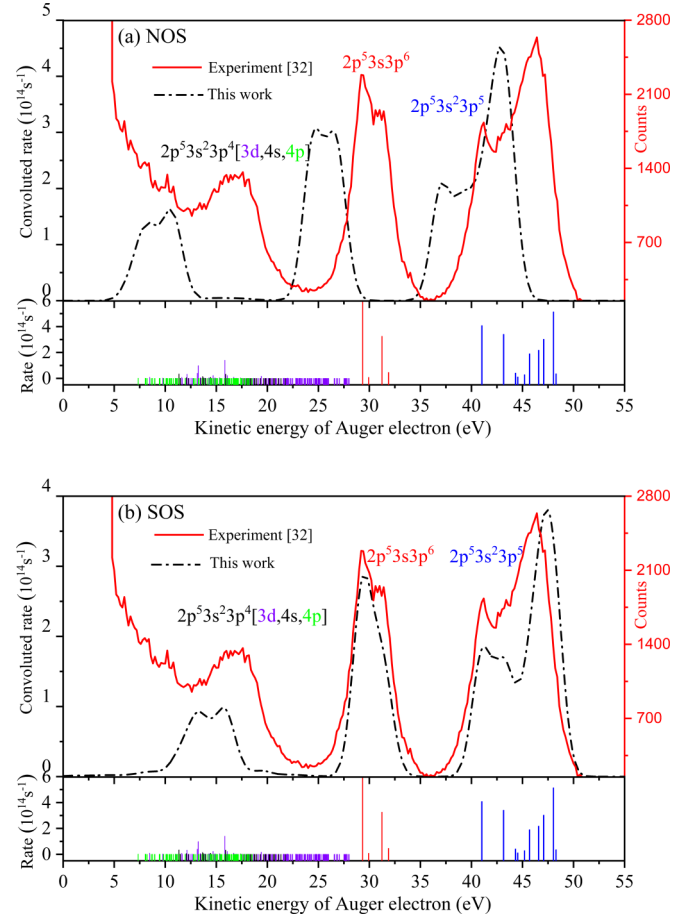


FIG. 3. The Coster-Kronig decay spectra for Ar⁺(2s⁻¹), calculated from the (a) NOS and (b) SOS, respectively. Both the theoretical spectra are convolved via a Gaussian profile of 2.25 eV FWHM to compare with the experimental results [32]. The vertical solid lines with different colors below the figure correspond to different final-state transition rates.

the relevant reference configurations ($2p^63s^23p^4$, $2p^63s3p^5$; $2p^53s^23p^5$, $2p^53s3p^6$) to active space of $3d$, $4s$, $4p$. In comparison with NOS, the main difference of SOS comes from the selection of orbital sets in obtaining Coster-Kronig final states.

The orbitals of NOS mutually are orthonormal with those of normal Auger of SOS, while not orthonormal with those of Coster-Kronig of SOS, as can be seen in Table I. The influence of orthonormality can be neglected, since the calculations of NOS and SOS are independent.

In order to check the convergence of SOS, i.e., make sure that the influence of further extending the CI is limited, more configurations in CI are added in SOS to get multiconfiguration SOS (MCSOS): the orbital sets of initial and final states are the same as SOS, but the CI are obtained by allowing valence orbitals $3s$, $3p$ single and double excitation from reference configurations Ar²⁺ $2p^53s^23p^5$, $2p^53s3p^6$ to active space of $3d$, $4s$, $4p$, $4d$, $5s$, $5p$. As listed in Table III, the rates of the two most important configurations $2p^53s^23p^5$, $2p^53s3p^6$ are 1.97×10^{15} and $0.99 \times 10^{15} \text{ s}^{-1}$, respectively, in MCSOS, which are very close to 2.09×10^{15} and $1.01 \times 10^{15} \text{ s}^{-1}$ in the SOS, respectively, signifying the SOS is roughly convergent.

TABLE III. Rates (A) and BRs for the Coster-Kronig SA calculated in the NOS and the SOS. To check the convergence of SOS, more configurations are added to the MCSOS calculation.

Ar ²⁺		NOS		SOS		MCSOS
Configuration	Level	$A(s^{-1})$	BR (%)	$A(s^{-1})$	BR (%)	$A(s^{-1})$
$2p^53s^23p^5$		2.35(15)	48.5	2.09(15)	56.6	1.97(15)
	¹ P ₁	4.18(13)	0.9	3.59(13)	1.0	3.51(13)
	³ D ₃	5.35(14)	11.0	5.13(14)	14.0	4.72(14)
	³ D ₂	2.97(14)	6.1	3.02(14)	8.2	2.85(14)
	³ S ₁	2.61(14)	5.4	2.18(14)	5.9	2.11(14)
	³ D ₁	6.14(13)	1.3	1.90(14)	5.2	1.78(14)
	³ P ₂	2.03(14)	4.2	2.87(13)	0.8	2.78(13)
	³ P ₀	6.39(13)	1.3	1.09(13)	0.3	1.07(13)
	³ P ₁	6.49(13)	1.3	4.07(13)	1.1	4.03(13)
	¹ D ₂	3.64(14)	7.5	3.40(14)	9.2	3.17(14)
	¹ S ₀	4.61(14)	9.5	4.07(14)	11.0	3.97(14)
$2p^53s3p^6$		1.51(15)	31.2	1.01(15)	27.4	0.99(15)
	³ P ₂	2.72(13)	0.6	4.61(13)	1.3	4.44(13)
	³ P ₁	5.87(14)	12.1	3.25(14)	8.8	3.12(14)
	³ P ₀	4.05(12)	0.1	8.11(12)	0.2	7.93(12)
	¹ P ₁	8.95(14)	18.5	6.30(14)	17.1	6.25(14)
$2p^53s^23p^43d$		7.00(14)	14.4	4.46(14)	12.1	
$2p^53s^23p^44s$		5.16(13)	1.1	1.08(14)	2.9	
$2p^53s^23p^44p$		2.24(14)	4.6	1.57(13)	0.4	
Total		4.85(15)	100	3.69(15)	100	

Since the choice of orbital sets in the SOS and NOS is the same in the normal Auger, the SOS's normal decay spectra are nearly the same as those of NOS displayed in Fig. 2. For the rates and BRs of SOS and NOS, listed in Table II, one can see the minute difference quantitatively, while for the Coster-Kronig decay shown in Fig. 3, the spectra obtained from SOS are in much better agreement with the experimental ones [32] compared to the results of NOS. The two foremost peaks around 30 and 45 eV correspond to the configurations $2p^53s3p^6$ and $2p^53s^23p^5$, respectively. The weaker peak around 15 eV mainly comes from the satellite of $2p^53s3p^6$ ($2p^53s^23p^43d$ and $2p^53s^23p^44s$), and below 15 eV, the intensities' difference between the SOS's spectra and those derived experimentally [32] are due to the background influence of experiment [32].

The transition rates and BRs for the Coster-Kronig decay states obtained from the NOS and SOS calculations are listed in Table III. The rates of paramount final states $2p^53s^23p^5$ are $2.43 \times 10^{15} s^{-1}$ and $2.09 \times 10^{15} s^{-1}$ in NOS and SOS, accounting for 48.5 and 56.6% of total rates, respectively. The rates for $2p^53s^23p^5$ level to level states are also represented, of which triplet state ³D₃ is the major ion yields. The second most important transition is $2p^53s3p^6$, of which singlet state ¹P₁ plays the main role. The $2p^53s^23p^43d$ and $2p^53s^23p^44s$ also contribute to the transition rates considerably. The experimental analysis [32] indicates that the

$2p^53s^23p^44p$ contribution is very small, which is in better agreement with the SOS's value of 0.4% than the NOS's value of 4.6%. In Table III, the rate difference of $2p^53s^23p^5$ between NOS and SOS is about 10%, while in $2p^53s3p^6$ the difference is about 50%; up to the $2p^53s^23p^44p$, the difference is about awful 14 times. Those signify that the smaller the energy difference between initial and final states, the more rates gap they have in NOS and SOS.

The total lifetime of the sum of normal Auger and Coster-Kronig decays with other experimental results, as listed in Table IV. The total transition rates (A) have the direct connection with the natural linewidth Γ and lifetime (τ)

$$\Gamma = \hbar A = \hbar / \tau = \sum_k \hbar A_{ik}. \quad (9)$$

The total lifetime of SOS with 0.26 fs is more close to the experimental values of 0.29 [32], 0.34 [28], 0.31 [42], 0.36 [5], and 0.29 fs [29] than that of NOS with 0.21 fs, which further verifies the reliability of the SOS's results. Therefore, the SOS will be analyzed elaborately in the following paper. The BR of 96.5% for Coster-Kronig decay states in the total Auger rates of SOS, means that the most ion yields of SA will decay to Arⁿ⁺ ($n \geq 3$), which will be discussed later.

B. Double Auger decay

The DA decay contains the direct and cascade processes. In the calculation of direct process, Ar⁺($2s^{-1}$) can decay to the bounds states of Ar³⁺ with the rate of $7.5 \times 10^{12} s^{-1}$, and to the autoionization states Ar³⁺ ($2p^53s^23p^4$) with $3.1 \times 10^{13} s^{-1}$, which can decay further to Ar⁴⁺. While in the cascade process, Ar⁺($2s^{-1}$) first decays to Ar²⁺ autoionization states, and then to Ar³⁺. Apparently, the rate of $3.85 \times 10^{13} s^{-1}$ from direct process is much smaller than the value of $3.69 \times 10^{15} s^{-1}$ from the cascade process. Therefore, the cascade process is highlighted below.

Our second Auger electron spectra shape from Ar²⁺ autoionization state decay to Ar³⁺, as shown in Fig. 4, are in good agreement with the results of experiment [32], which further validate the method of the cascade.

In addition, Lablanquie *et al.* [32] also gave the DA spectra from Ar⁺($2s^{-1}$) decay to Ar³⁺, which are compared with the theoretical results, exhibited in Fig. 5. In consideration of the correlation energy variant in each ion state, the electron spectra are shifted 2 eV toward lower energy to match the experimental ones [32]. The total Auger spectra are the sum of the intermediate state Ar²⁺ $2p^53s^23p^5$, $2p^53s3p^6$, and $2p^53s^23p^4nl$ ($nl = 3d, 4s, 4p$). The intermediate states Ar²⁺ $2p^53s^23p^5$ mainly decay to Ar³⁺ $3s^23p^3$, the Ar²⁺ $2p^53s3p^6$ to Ar³⁺ $3s3p^4$, and the Ar²⁺ $2p^53s^23p^4nl$ ($nl = 3d, 4s, 4p$) to Ar³⁺ $2p^53s^23p^4nl$ ($nl = 3d, 4s, 4p$). In this step of cascade, mainly one $3p$ valence electron fills the $2p$ hole, leading to the emission of another $3p$ electron. In addition, the left of

TABLE IV. The total lifetime τ (fs) of Ar⁺($2s^{-1}$) Auger decay in NOS and SOS, along with the experimental values.

This work (fs)		Experimental values (fs)	
0.21 (NOS)	0.26 (SOS)	0.29 [32], 0.34 [28], 0.31 [42], 0.36 [5], 0.29 [29]	

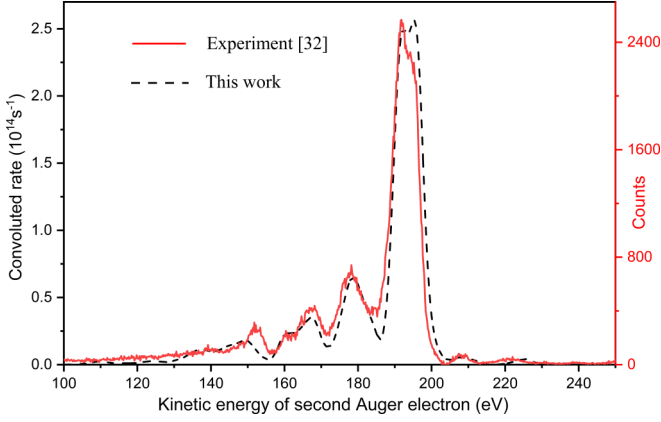


FIG. 4. The Auger spectra of the second step of the cascade process, i.e., the decay from Ar^{2+} to Ar^{3+} . Theoretical spectra are convoluted with a Gaussian profile of 3.5 eV FWHM and shifted 2 eV toward left (lower energy).

vertical blue solid line is autoionization states, such as states of $3s3p^3nl$ ($nl = 3d, 4s, 4p$).

The detailed analysis for the transition rates and BRs of Ar^{3+} ion states are listed in Table V. The two major configurations are $3s^23p^3$ and $3s3p^4$, accounting for 36.1 and 29% of the total rates, respectively. The contribution of $3s^23p^23d$ is also important, accounting for 12.7% for their strong mixing with $3s3p^4$. In addition, it can be inferred that the sum of $3s3p^3nl$ ($nl = 3d, 4s, 4p$) is 7.5%, part of which will populate the Ar^{4+} ion yields, as shown in Fig. 5.

C. Triple Auger decay

The $\text{Ar}^+(2s^{-1})$ can further decay to Ar^{4+} with the emission of three electrons, forming the triple Auger (TA) decay process

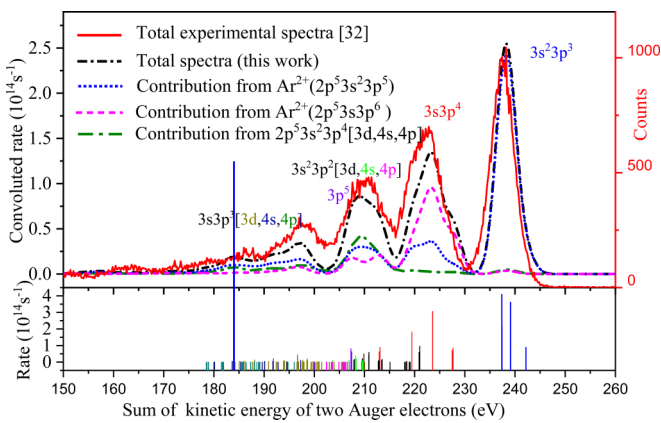
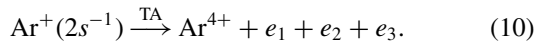
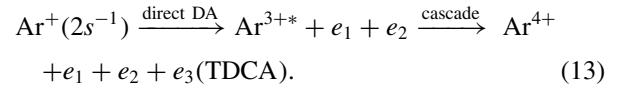
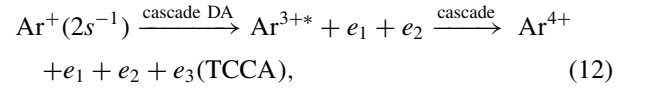
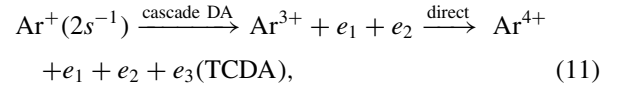


FIG. 5. Comparison of the DA spectra for $\text{Ar}^+(2s^{-1})$ decay to Ar^{3+} . Our total and different Ar^{2+} configuration theoretical spectra are convoluted with a Gaussian profile of 4 eV FWHM and shifted 2 eV toward left (lower energy). The vertical solid lines with different colors below the figure correspond to different final-state transition rates, and the vertical blue solid line is the threshold of Ar^{3+} .

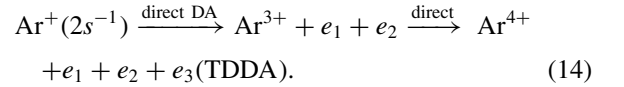
TABLE V. Transition rates (A) and BRs for the main transition configurations of DA decay from the $\text{Ar}^+(2s^{-1})$. The numbers in parentheses denote powers of 10.

Configuration (Ar^{3+})	$A(s^{-1})$	BR (%)
$3s^23p^3$	1.32(15)	36.1
$3s3p^4$	1.06(15)	29.0
$3p^5$	1.96(14)	5.4
$3s^23p^23d$	4.63(14)	12.7
$3s^23p^24s$	1.17(14)	3.2
$3s^23p^24p$	4.17(12)	0.1
$3s3p^33d$	2.13(14)	5.9
$3s3p^34s$	5.46(13)	1.5
$3s3p^34p$	4.39(12)	0.1
Total	3.64(15)	100

It also can be explained by the cascade and direct TA processes. The cascade TA process includes at least one cascade process, which can be summarized as



In the direct TA process, three Auger electrons are emitted simultaneously and can be given by



The Ar^{3+} with and without the asterisk denote the autoionization states and bound states, respectively. Multistep approach is proposed to account for Eqs. (11)–(14). For instance, in the TCDA, two electrons (e_1 and e_2) are ejected via the cascade DA decay first; then, the second electron (e_2) ionizes a bound electron (e_3) via the direct process. The TCDA consists of two parts: the cascade DA combined with the KO process (TCKO) and SO process (TCSO), respectively. Equation (12), i.e., TCCA, is the combination of cascade DA and cascade processes. Similarly, in Eq. (13), the final states of Ar^{3+*} will decay to Ar^{4+} following the direct process from Ar^+ to Ar^{3+*} . The rates for TCKO, TCSO, TCCA, and TDCA are given in the following:

$$A_{if}^{\text{TCKO}} = \sum_m A_{im}^{\text{SA}} \Gamma_m^{-1} \sum_c A_{mc}^{\text{SA}} \Omega_{cf}(\varepsilon_{mc}), \quad (15)$$

$$A_{if}^{\text{TCSO}} = \sum_m A_{im}^{\text{SA}} \Gamma_m^{-1} \sum_c A_{mc}^{\text{SA}} |\langle \psi_f^{2+} \kappa; J_T M_T | \psi_c^+ \rangle|^2, \quad (16)$$

$$A_{if}^{\text{TCCA}} = \sum_m A_{im}^{\text{SA}} \Gamma_m^{-1} \sum_c A_{mc}^{\text{SA}} \Gamma_c^{-1} A_{cf}^{\text{SA}}, \quad (17)$$

$$A_{if}^{\text{TDCA}} = \sum_m A_{im}^{\text{SA}} \Omega_{mc}(\varepsilon_{im}) \Gamma_c^{-1} A_{cf}^{\text{SA}}. \quad (18)$$

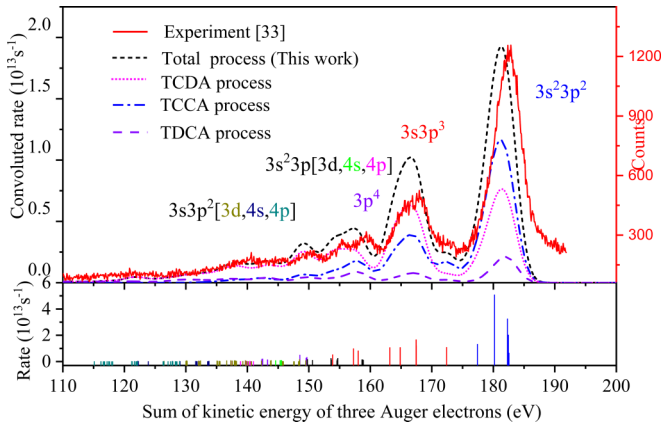


FIG. 6. Theoretical TA spectra are shifted about 3.25 eV toward low kinetic energy to compare with the experimental [33] spectra. The spectra lines in exception of the red experimental line correspond to TCDA, TCCA, TDCA, and total decay processes, respectively. The vertical solid lines with different colors below the figure correspond to different final-state transition rates.

In Eq. (15), Γ_m stands for the total width of specific states Ar^{2+} , the A_{mc}^{SA} denotes the rate from the intermediate states Ar^{2+} to the next intermediate states Ar^{3+} , $\Omega_{cf}(\varepsilon_{mc})$ is the collision strength of the inelastic scattering upon “the second intermediate” Auger electron to the final states Ar^{4+} . The same analysis can be applied to Eqs. (16)–(18). Noted in the first step of the TDCA process only the KO mechanism is included, for the minor contribution of the SO. On the other hand, in the direct process from Ar^+ to Ar^{4+} , the contribution of Eq. (14) is so minor as to be negligible. In summary, the TA decay can be described by the sum of TCDA (including TCKO and TCSO), TCCA, and TDCA processes.

In Fig. 6, theoretical TA spectra including TCDA, TCCA, and TDCA processes agree well with the experimental [33] results. The main peaks are indicated with different main configurations. Around 180 eV of three Auger electrons corresponding to the ground states, TCCA plays the main role in the total spectra, TCDA is second most important, then

TDCA, while below 175 eV corresponding to the other configurations, the main contribution comes from TCDA, and with the further decrease of kinetic energy, the contribution of TCDA increases.

To analyze the detailed contributions, the transition rates and BRs of Ar^{4+} ion states, including the TCDA, TCCA, and TDCA processes, are listed in Table VI. The rates of TA decay are the sum of TCDA with $1.4 \times 10^{14} \text{ s}^{-1}$, TCCA with $1.2 \times 10^{14} \text{ s}^{-1}$, and TDCA with $3.1 \times 10^{13} \text{ s}^{-1}$. In the TCDA process, the contribution of TCKO with rates $1.4 \times 10^{14} \text{ s}^{-1}$ is much greater than that of TCSO with rates $6.5 \times 10^{12} \text{ s}^{-1}$ by at least an order of magnitude, indicating that the TCKO mechanism is prominent. The paramount configuration contribution to total TCDA rates come from the $3s^2 3p^3$ with the rates of $5.6 \times 10^{13} \text{ s}^{-1}$, accounting for 38.6%. The second most important transitions originate from the ground state $3s^2 3p^2$ with the rates of $5.6 \times 10^{13} \text{ s}^{-1}$ and BR of 31%. Apart from $3s^2 3p^3$ and $3s^2 3p^2$, the $3p^4$, $3s^2 3p^3d$, and $3s^2 3p^2 3d$ are also important; their rates are all greater than 10^{13} s^{-1} . In the TCCA process, the paramount configuration contribution comes from the $3s^2 3p^2$ with the rates of $6.8 \times 10^{13} \text{ s}^{-1}$; the second important transition is $3s^2 3p^3$ with rates $3.8 \times 10^{13} \text{ s}^{-1}$, which are reversed in the TDCA process in that the rates contribution of $3s^2 3p^3$ is maximal. The rates of $3s^2 3p^2$ and $3s^2 3p^3$ are nearly larger by one order of magnitude than that of all other configurations. For the TDCA process, the configuration $3s^2 3p^2$ and $3s^2 3p^3$ account for the BRs of 35 and 31.6% of total TDCA rates, respectively. The configuration $3s^2 3p^2 3d$ with the BR of 14.2% also has an important contribution. In short, the $3s^2 3p^3$ and $3s^2 3p^2$ contribute most to the total TA.

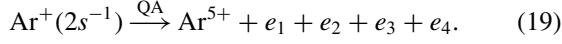
The TCCA is the most important process in the experiment of Lablanquie *et al.* [32], which is not in accord with the analysis here that the TCDA is more important than the TCCA process. However, Lablanquie *et al.* [33] observed the TA decay once again did not clarify which process was significant. It is noted that the TDCA process which was not mentioned by Lablanquie *et al.* [32,33] but manifested in Ref. [31] also has a certain contribution. On the other hand, the sum for TCCA and TDCA with $1.51 \times 10^{14} \text{ s}^{-1}$ in the cascade process is slightly bigger than the TCDA with $1.4 \times 10^{14} \text{ s}^{-1}$. Further experimental analysis is expected.

TABLE VI. Transition rates (A) and BRs for major configurations in Ar^{4+} ions. TCDA (TCKO and TCSO), TCCA, and TDCA processes are included. The numbers in parentheses denote powers of 10.

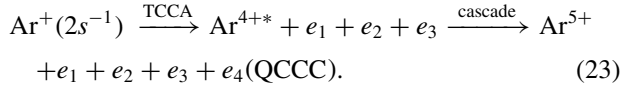
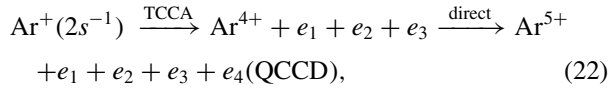
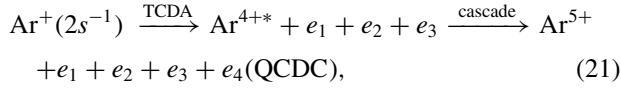
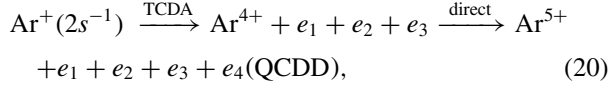
Ar ⁴⁺	A(s ⁻¹)						BR (%)			
	TCKO	TCSO	TCDA	TCCA	TDCA	Total	TCDA	TCCA	TDCA	Total
$3s^2 3p^2$	4.3(13)	1.7(12)	4.5(13)	6.8(13)	1.1(13)	1.2(14)	31.0	57.8	35	42.0
$3s^2 3p^3$	5.3(13)	2.5(12)	5.6(13)	3.8(13)	9.8(12)	1.0(14)	38.6	32.5	31.6	35.6
$3p^4$	1.1(13)	6.3(11)	1.2(13)	3.5(12)	2.5(12)	1.6(13)	8.2	3.0	8.1	5.6
$3s^2 3p^3d$	9.6(12)	3.6(11)	1.0(13)	5.4(12)	9.8(11)	1.6(13)	6.9	4.6	3.2	5.6
$3s^2 3p^4s$	2.5(12)	1.4(11)	2.7(12)	2.7(11)	4.2(9)	3.0(12)	1.8	0.2	0.01	1.0
$3s^2 3p^4p$	1.2(12)	6.6(10)	1.2(12)	2.1(11)	2.5(10)	2.2(12)	0.9	0.2	0.08	0.8
$3s^2 3p^2 3d$	1.1(13)	5.6(11)	1.1(13)	1.7(12)	4.4(12)	1.8(13)	7.9	1.5	14.2	6.2
$3s^2 3p^2 4s$	2.4(12)	1.8(11)	2.5(12)	2.1(10)	3.2(10)	2.7(12)	1.7	0.02	0.1	0.9
$3s^2 3p^2 4p$	7.8(11)	5.7(10)	8.3(11)	1.3(10)	1.2(11)	1.1(12)	0.6	0.01	0.4	0.3
All	1.4(14)	6.5(12)	1.4(14)	1.2(14)	3.1(13)	2.9(14)	100	100	100	100

D. Quadruple Auger decay

Some TA final states can further decay to Ar^{5+} , forming the quadruple Auger decay (QA). The whole QA can be described as



Based on the analysis of DA and TA process, we mainly consider the following processes:



The Ar^{4+} with and without the asterisk in Eqs. (20)–(23) denote the autoionization states and bound states, respectively. The multistep approach is suggested to cope with Eq. (20), which is deemed as a KO process following the TCDA, due to the small contribution of SO process. In the QCDD process, two electrons (e_1 and e_2) are ejected sequentially by the cascade DA decay first, then the second electron e_2 ionizes a bound electron (e_3) by inelastic scattering; further, one of Auger electrons (e_2 or e_3) as incident electron ionizes another bound electron (e_4), i.e., the last three electrons are ejected simultaneously. A similar analysis is applied to the QCDC process. The Ar^{3+} ion yield populated from Eqs. (22) and (23), lying above the ground state of Ar^{5+} , is nearly zero, meaning that for Ar^{5+} the ion yield of Eqs. (22) and (23) are negligible.

The rates of QCDD and QCDC can be obtained from the expression

$$A_{if}^{\text{QCDD}} = \sum_m A_{im}^{\text{SA}} \Gamma_m^{-1} \sum_c A_{mc}^{\text{SA}} \Omega_{cd}(\varepsilon_{mc}) \times \int_0^{E_{\max}} \rho_{cd}(\varepsilon) \Omega_{df}(\varepsilon) d\varepsilon, \quad (24)$$

$$A_{if}^{\text{QCDC}} = \sum_m A_{im}^{\text{SA}} \Gamma_m^{-1} \sum_c A_{mc}^{\text{SA}} \Omega_{cd}(\varepsilon_{mc}) \sum_d A_{df}^{\text{SA}} \Gamma_d^{-1}. \quad (25)$$

In Eq. (24), $A_{mc}^{\text{SA}} \Omega_{cd}(\varepsilon_{mc})$ is the rates of direct DA decay from the intermediate state Ar^{2+} with energy E_m to the intermediate state of Ar^{4+} ion with energy E_d . Two “intermediate” Auger electrons sharing the total energy ($E_{\max} = E_m - E_d$) are emitted. The utilization of binary-encounter dipole model [43] suggests that the normalized distribution $\rho_{cd}(\varepsilon)$ is an asymmetrical U-shape distribution, which consists of a fast Auger electron and a slow Auger electron. The validity of the

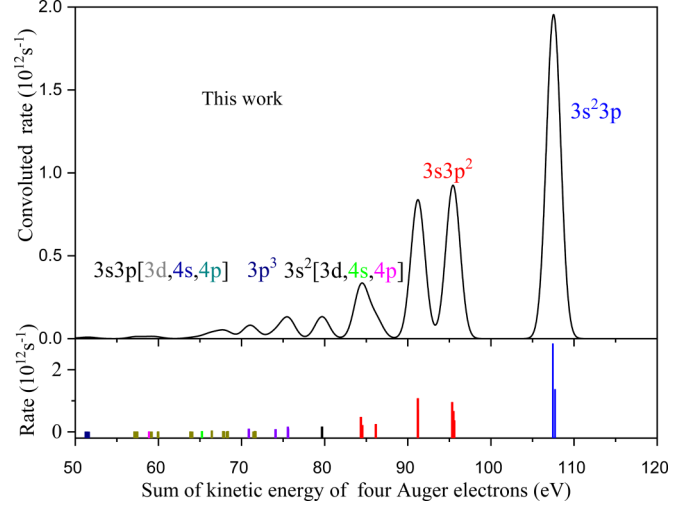


FIG. 7. Theoretical QA spectra convolved with a Gaussian profile of 2 eV FWHM from $\text{Ar}^+(2s^{-1})$ decay to Ar^{5+} . The vertical solid lines with different colors below the figure correspond to different final-state transition rates.

BE model has been verified in Refs. [11,41]. $\Omega_{df}(\varepsilon)$ is the collision strength of inelastic scattering off a bound electron in the intermediate Ar^{4+} ion states by one of the two intermediate Auger electrons. Similarly, the rates of QCDC process can be obtained.

Due to the lack of experimental spectra, to our knowledge, only the QA spectra are exhibited in Fig. 7. By and large, the ion yields decrease with the decrease of four Auger electron energy. The characteristic data on the QA decay of the $\text{Ar}^+(2s^{-1})$ including the contribution of QCDD primarily and QCDC fractionally (nearly 1/40 of QCDD) are given in Table VII. The ground and first excited states $3s^2 3p$ and $3s 3p^2$ occupy nearly 90% of all rates, while the rest of the other states take up 10%.

E. Ion yields

Our ion yield ratios for the SA, DA, TA, and QA decay of $\text{Ar}^+(2s^{-1})$, together with other theoretical and experimental data, are listed in Table VIII. Based on the NOS of Ar^{2+} , we also calculated its ion yield ratios, to compare with the ratios

TABLE VII. Similar to Table VI but for major configurations of Ar^{5+} ion states including QCDD and QCDC processes.

Configuration (Ar^{5+})	$A(s^{-1})$	BR (%)
$3s^2 3p$	4.2(12)	42.0
$3s 3p^2$	4.7(12)	47.0
$3p^3$	4.8(11)	4.8
$3s^2 3d$	2.8(11)	2.8
$3s^2 4s$	1.9(10)	0.2
$3s^2 4p$	9.3(9)	0.1
$3s 3p 3d$	2.7(11)	2.7
$3s 3p 4s$	1.3(10)	0.1
$3s 3p 4p$	3.6(9)	0.04
All	1.0(13)	100

TABLE VIII. Ion yield ratios (%) of single Auger (SA), double Auger (DA), triple Auger (TA), and quadruple Auger (QA) decay, in the NOS and SOS, together with other theoretical and experimental data. The contribution of TA including the TCCA, TCDA, and TDCA decays, is also listed respectively.

Ar ⁺ (2s ⁻¹)	This work		Experiment		Theory		
	NOS	SOS	Lablanquie (2011) [32]	Brünken (2002) [31]	Kasstra (1993) [30]	Lablanquie [32]	Kochur (1995) [16]
SA	2.7	3.5	3.0	1.0(4)	3.6	5.0	4.2
DA	76.7	88.7	89.0	89.0(3)	96.4	95.0	93.4
TA	20.4	7.5	8.0	10.0(2)			2.5
TCCA	16.8	3					
TCDA	2.8	3.7					
TDCA	0.8	0.8					
QA	0.2	0.26	0.3				0

of SOS and experiments. In the NOS, except for the ratio of 2.7% in SA decay in agreement with those experimental values [31,32], the DA ratio of 76.7% is obviously smaller than all the other experimental and theoretical values, and the TA ratio of 20.4% dramatically is twice more than those experimental values of 8.0% [32] and 10.0% [31], respectively.

In the SOS, the decay ratios (Ar²⁺ : Ar³⁺ : Ar⁴⁺ = 3.5 : 88.7 : 7.5) are quite close to the recent experimental data (3.0:89.0:8.0) [32]. The TA decay ratio of 7.5% is in much better agreement with the experimental one of 8.0% [32] than the Kochur *et al.* theoretical value of 2.5%. The detailed investigation shows that the TA ion yields come from three different but important decay processes: TCDA, TDCA, and TCCA with 3, 3.7, and 0.8%, respectively, while in Ref. [16], the TCDA and TDCA processes are not included. On the other hand, the overestimates of SA (5%) and DA (95%) of their theoretical results in Ref. [32], and the SA (3.6%) and DA (96.4%) [30] are due to the absence of TA and QA decays in the calculation. Obviously, they [30,32] did not discuss the triple and quadruple Auger decay, and the triple Auger involving the direct process and quadruple Auger were not discussed in theory [16]. Furthermore, the investigation of the QA decay process of Ar⁺(2s⁻¹) provides a more stringent test for the SOS calculation, and the ratio of 0.26% compared with the experimental value of 0.3% [32] is quite satisfactory.

IV. CONCLUSION

The complete Auger processes of Ar⁺(2s⁻¹) including SA, DA, TA, and QA decays are investigated, based on many-body perturbation theory. The spectra, lifetime, and ion yield ratios from level to level rates are in good agreement with those of experiments. The results show that the Coster-Kronig process

is prominent for the SA decay, which is in accord with the observations of Lablanquie *et al.* [32,33] and Brünken *et al.* [31]. In the DA decay with a ratio of 88.7% of total Auger decay rates, the cascade mechanism plays the main role. Our TA decay ratio of 7.5% is in line with Lablanquie's value of 8.0% [32,33] and Brünken's value of 10.0% [31] when we take the complex decay processes including the TCDA, TDCA, and TCCA into consideration completely. Further, based on the analysis of TA, we get the QA decay ratio of 0.26%, which fairly agrees with the value of 0.3% [32,33].

In summary, the good agreement between theoretical and experimental results demonstrates that the multistep approach is effective to investigate the MA decay for Ar⁺(2s⁻¹). In addition, the vastly different results obtained in NOS and SOS profoundly manifest that it is crucial to select separate orbital sets of configurations to obtain accurate ASFs in the Auger decay of Ar⁺(2s⁻¹). It also signifies that our approach in optimizing the orbitals is different from that of other Auger decay such as Ar 2p⁻¹4s [10], due to different main decay processes. The studies show that these approaches should also be useful in dealing with other deep holes of Auger decay such as Kr (1s, 2s, 2p, 3s, and 3p core hole) [13–17] and Xe (1s, 2s, 2p, 3s, 3p, 3d, 4s, and 4p hole) [12,18–20].

ACKNOWLEDGMENTS

We would like to thank Prof. Pascal Lablanquie for providing the experimental data in Refs. [32,33]. This work is supported by the National Key Research and Development Program of China (Grant No. 2017YFA0402300), and the National Natural Science Foundation of China (Grants No. 11774344 and No. 11474033).

- [1] J. Viefhaus *et al.*, *Phys. Rev. Lett.* **92**, 083001 (2004).
 [2] T. A. Carlson and M. O. Krause, *Phys. Rev. Lett.* **14**, 390 (1965).
 [3] M. Y. Amusia, I. S. Lee, and V. A. Kilin, *Phys. Rev. A* **45**, 4576 (1992).
 [4] S. M. Huttula *et al.*, *Phys. Rev. Lett.* **110**, 113002 (2013).
 [5] W. Mehlhorn, *Z. Phys.* **208**, 1 (1968).
 [6] A. Müller *et al.*, *Phys. Rev. Lett.* **114**, 013002 (2015).

- [7] W. Bambynek, B. Crasemann, R. W. Fink, H. U. Freund, H. Mark, C. D. Swift, R. E. Price, and P. V. Rao, *Rev. Mod. Phys.* **44**, 716 (1972).
 [8] F. Penent, J. Palaudoux, P. Lablanquie, L. Andric, R. Feifel, and J. H. D. Eland, *Phys. Rev. Lett.* **95**, 083002 (2005).
 [9] S. Stock, R. Beerwerth, and S. Fritzsche, *Phys. Rev. A* **95**, 053407 (2017).

- [10] Y. Ma, Z. Liu, F. Zhou, and Y. Qu, *Phys. Rev. A* **98**, 043417 (2018).
- [11] Y. Ma, F. Zhou, L. Liu, and Y. Qu, *Phys. Rev. A* **96**, 042504 (2017).
- [12] Y. Hikosaka, P. Lablanquie, F. Penent, T. Kaneyasu, E. Shigemasa, J. H. D. Eland, T. Aoto, and K. Ito, *Phys. Rev. A* **76**, 032708 (2007).
- [13] J. Palaudoux, P. Lablanquie, L. Andric, J. H. D. Eland, and F. Penent, *J. Phys. Conf. Ser.* **141**, 012012 (2008).
- [14] V. Jonauskas, R. Karazija, and S. Kučas, *J. Phys. B.* **41**, 215005 (2008).
- [15] Y. Morishita, Y. Tamenori, K. Okada, T. Oyama, K. Yamamoto, K. Tabayashi, T. Ibuki, K. Moribayashi, and I. H. Suzuki, *J. Phys. B.* **39**, 1323 (2006).
- [16] A. G. Kochur, V. L. Sukhorukov, A. I. Dudenko, and P. V. Demekhin, *J. Phys. B.* **28**, 387 (1995).
- [17] A. El-Shemi, Y. Lofty, and G. Zschornack, *J. Phys. B.* **30**, 237 (1997).
- [18] T. Hayaishi, E. Murakami, Y. Lu, E. Shigemasa, A. Yagishita, F. Koike, and Y. Morioka, *Phys. Rev. A* **54**, 4064 (1996).
- [19] J. H. D. Eland, C. Slater, S. Zagorodskikh, R. Singh, J. Andersson, A. Hult-Roos, A. Lauer, R. J. Squibb, and R. Feifel, *J. Phys. B.* **48**, 205001 (2015).
- [20] M. N. Piancastelli, K. Jänkälä, L. Journal, T. Gejo, Y. Kohmura, M. Huttula, M. Simon, and M. Oura, *Phys. Rev. A* **95**, 061402(R) (2017).
- [21] Y. Ma, F. Zhou, Z. Liu, and Y. Qu, *Chin. Phys. B* **27**, 063201 (2018).
- [22] L. Liu, Y. Li, C. Gao, and J. Zeng, *Phys. Rev. A* **101**, 012507 (2020).
- [23] J. M. Sampaio, T. I. Madeira, M. Guerra, F. Parente, J. P. Santos, P. Indelicato, and J. P. Marques, *Phys. Rev. A* **91**, 052507 (2015).
- [24] T. A. Carlson and M. O. Krause, *Phys. Rev. Lett.* **17**, 1079 (1966).
- [25] T. Lanz, K. Cunha, J. Holtzman, and I. Hubeny, *Astrophys. J.* **678**, 1342 (2008).
- [26] X. M. Zhu and Y. K. Pu, *J. Phys. D: Appl. Phys.* **43**, 403001 (2010).
- [27] H. J. N. van Eck, T. A. R. Hansen, A. W. Kleyn, H. J. van der Meiden, D. C. Schram, and P. A. Zeijlmans van Emmichoven, *Plasma Sources Sci. Technol.* **20**, 045016 (2011).
- [28] P. Glans, R. E. LaVilla, M. Ohno, S. Svensson, G. Bray, N. Wassdahl, and J. Nordgren, *Phys. Rev. A* **47**, 1539 (1993).
- [29] T. Kylli *et al.*, *Phys. Rev. A* **59**, 4071 (1999).
- [30] J. S. Kasstra and R. Mewe, *Astron. Astrophys. Suppl. Ser.* **97**, 443 (1993).
- [31] S. Brünken, Ch. Gerth, B. Kanngießer, T. Luhmann, M. Richter, and P. Zimmermann, *Phys. Rev. A* **65**, 042708 (2002).
- [32] P. Lablanquie *et al.*, *Phys. Chem. Chem. Phys.* **13**, 18355 (2011).
- [33] P. Lablanquie *et al.*, *J. Electron Spectrosc. Relat. Phenom.* **220**, 125 (2017).
- [34] F. Penent, P. Lablanquie, R. I. Hall, J. Palaudoux, K. Ito, Y. Hikosaka, T. Aoto, and J. H. D. Eland, *J. Electron Spectrosc. Relat. Phenom.* **144-147**, 7 (2005).
- [35] K. G. Dyall and F. P. Larkins, *J. Phys. B.* **15**, 4103 (1982).
- [36] M. F. Gu, *Can. J. Phys.* **86**, 675 (2008).
- [37] S. Fritzsche, *Comput. Phys. Commun.* **183**, 1525 (2012).
- [38] P. Jönsson, X. He, C. F. Fischer, and I. P. Grant, *Comput. Phys. Commun.* **177**, 597 (2007).
- [39] S. Fritzsche, B. Fricke, and W. D. Sepp, *Phys. Rev. A* **45**, 1465 (1992).
- [40] S. Fritzsche, J. Nikkinen, S. M. Huttula, H. Aksela, M. Huttula, and S. Aksela, *Phys. Rev. A* **75**, 012501 (2007).
- [41] F. Zhou, Y. Ma, and Y. Qu, *Phys. Rev. A* **93**, 060501(R) (2016).
- [42] R. Püttner, P. Holzhey, M. Hrast, M. Zitnik, G. Goldsztejn, T. Marchenko, R. Guillemin, L. Journal, D. Koulentianos, O. Travnikova, M. Zmerli, D. Ceolin, Y. Azuma, S. Kosugi, A. F. Lago, M. N. Piancastelli, and M. Simon, *Phys. Rev. A* **102**, 052832 (2020).
- [43] Y.-K. Kim and M. E. Rudd, *Phys. Rev. A* **50**, 3954 (1994).